ENERGY MANAGEMENT-BASED DESIGN OF A WANKEL HYBRID-ELECTRIC UAV

Teresa Donateo, Claudia Lucia de Pascalis, Antonio Ficarella

Università del Salento, Dipartimento di Ingegneria dell'Innovazione (Department of Engineering for Innovation), via per Monteroni, 73100, Lecce, Italy

Corresponding author: Teresa Donateo (teresa.donateo@unisalento.it), +39 0832 297 754

Abstract

Purpose: The goal of this investigation is the optimization of design and energy management in a parallel hybrid-electric powertrain to replace the conventional engine of an existing tactical Unmanned Aerial Vehicle (UAV) equipped with a Wankel engine with a pre-defined flight mission. The proposed powertrain can work in four different operating modes: electric, thermal, power-assist and charging.

Methodology: The power request at propeller axis of each flight segment is used as input for an in-house model that calculates the overall fuel consumption throughout the mission (M_{fuel}) and the maximum payload weight (W_{pay}) by means of an average-point analysis. These outputs depend on the energy management strategy that is expressed by the power-split ratio between engine and electric phase (U_{phase}) of each mission phase, according to which the components of the hybrid system are sized. The in-house model is integrated into an optimization framework to find the optimal set of U_{phase} and battery size that minimizes M_{fuel} and maximize W_{pay}.

Findings: It was found a 3.24% saving of the fuel mass burned throughout the mission (or, alternative an improvement of endurance by 4.3%) with about the same maximum-payload mass (+0.2%) of the original configuration, or a smaller fuel saving with +11% more payload. The fuel saving of 3.24% corresponds to -3.25% in total emissions of CO_2 and a 2.34% reduction of the cost-per-mission.

Practical Implication:

This study demonstrates that environmental advantages, even if limited, can be already obtained from optimal design and management of the hybrid power system with today technologies, while waiting for further benefits from the introduction of advanced technologies for batteries and electric machines.

Originality: The main novelties are the design of the powertrain on the basis of the energy management and the application of scalability and hybridization to Wankel engines.

Keywords

Hybrid electric aircraft. UAV. Energy management strategy. Wankel engine. Scaling models.

Introduction

In 2010 the International Civil Aviation Organization (ICAO) established new certification standards for the reduction of noise and emissions to be reached by different time steps (International Civil Aviation Organization, 2010). This inevitably led the scientific community to step up efforts in this direction. One of the possible ways (Brelje et al., 2019) is the electrification of the power systems that allows higher power-to-weight ratios, reliability, compactness, quietness and, above all, pollutant emissions cutback, with respect to the conventional engine configurations.

Electric architectures for aircraft propulsion can be divided into four main configurations: full-electric, turbo-electric, series hybrid-electric, and parallel hybrid-electric. For large aircraft such as commercial planes, full-electric propulsion will be possible only when new technologies will be available for batteries and electrical machines (Fletcher et al., 2016). On the contrary, it is already feasible for small and medium unmanned aerial vehicles (UAVs) or for few-seat aircraft like the Airbus E-Fan and the Pipistrel Alpha Electro. Turbo-electric propulsion is being studied together with new aircraft concepts for large and heavy aircraft, some examples are NASA's N3-X and STARC-AB. Series and parallel hybrid-electric architectures can be suitable for aircraft belonging to the FAA's categories of small and medium weight.

Pornet et al., 2015 classified electrified power systems in terms of energy and power hybridization factors. In particular, the power hybridization factor is defined as:

$$HF = \frac{P_{EM}}{P_{TOT}} = \frac{P_{EM}}{P_{ICE} + P_{EM}} \tag{1}$$

where P_{EM} is the power delivered by the motor, P_{ICE} is the power from the engine, and P_{TOT} is the total quantity of mechanical power generated by the hybrid architecture). Similarly, an energy hybridization factor can be defined as:

$$HE = \frac{E_{batt}}{E_{tot}} = \frac{E_{batt}}{E_{batt} + E_{fuel}} \tag{2}$$

where E_{batt} is the energy stored in the battery, E_{fuel} is the energy content of the fuel tank.

Previous investigations of the authors demonstrated that large improvements can be obtained by exploiting synergies between powertrain, aircraft structure, and mission during the design process of electric and hybrid-electric aircraft (Donateo et al., 2018). This is even truer if new powerful concepts are involved in the design process, such as, multi-functionalization, distributed propulsion, etc. In this framework, it is not possible for the aircraft design process to remain the same (Moore et al., 2014), because the benefits of the new technologies could not be fully exploited. Advanced genetic algorithms were found in previous studies to be a precious tool in this kind of application (Donateo et al. 2019). In

fact, they allow taking into account several metrics or optimization goals (like fuel economy, electric endurance, performance indexes, etc.,) and a large number of input parameters (including aircraft specification, flight conditions, architecture, size of converters and storage systems, hybridization factor, energy management strategies and so on). As a step further in the previous approach, this investigation focuses on the key role of energy management in hybrid electric systems, which is called to decide, at each step of the mission, how to use the energy stored in the battery.

Energy management strategies can be classified into four categories (Serrao, 2009): numerical optimization, analytic optimal control theory, instantaneous optimization and heuristic control techniques. Heuristic Control Techniques are rule-based and require a very low computational cost. The need of advanced control strategies in the automotive field is linked to the extreme variability and unpredictability of driving conditions. On the contrary, the flight conditions of an aircraft are much more controllable so the energy management can be performed in an easier way.

To exploit the synergy between configuration and energy management, it is possible to consider four approaches (Silvas et al. 2016). In the “Design-First-Then-Control” approach, the architecture is set a priori and then the control management is optimized. This approach is made recursive in the “Alternated design-control optimization” where the management strategy optimized at each step is used for the optimization of the design in the next step. In the “nested approach” for each evaluation of a plant, a full optimization of the controller design is performed. In the “Simultaneous design-control optimization approach” a simultaneous optimization of plant and controller is performed. Some examples of the first approach applied to aircraft can be found in literature (Harmon et al. 2005, Pornet et al. 2015).

The approach considered in this study belongs to the type “Simultaneous design-control optimization approach” and differs from the method previously proposed (Donateo et al., 2018) in some aspects. The first one is the usage of a simulation approach more suitable to the aircraft field. In fact, the mission is not discretized into small time steps (like in the automotive case) but subdivided in phases and segments. The total request of mechanical power (i.e. the power required at propeller axis) at each segment is given as input to an energy model that returns the overall fuel consumption throughout the mission (M_{fuel}) and the maximum payload weight (W_{pay}) by means of an average-point analysis. The second novelty is that the powertrain configuration is shaped during the calculation as a function of the energy management strategy. Since the idea is to substitute the power system of an existing aircraft, the optimization starts form a baseline configuration and is run with the constraint of keeping the same take-off weight of the baseline configuration. The optimization tool used in this study is the S-Metric Selection Evolutionary Multi-Objective Algorithm (SMS-EMOA) by Emmerich et al. (2005) that was modified by the authors in order to include a constraint handling strategy.

In short, this study defines a method of sizing parallel hybrid-electric power systems for UAVs (or aircraft, in general) involving the optimization of the energy management strategy throughout the mission by means of multi-objective evolutionary algorithms. The method is here applied to a tactical UAV with an installed power below 70kW, an application

where Wankel engines are preferred. Therefore, another novelty of this investigation is the development of a model able to estimate the fuel consumption in each mission segment according, not only to the flight conditions of the segment, but also to the size of the Wankel engine.

The paper is organized as follows. It starts with the specification of the UAV power system followed by the description of the energy modes of the parallel hybrid electric architecture. The third section explains the design methodology whose results are then discussed in the fourth section also in terms of economic and environmental benefits by comparing the original and the optimal configurations found in the optimization.

Hybridization of a tactical UAV

The tactical UAV considered in this investigation is a Medium Altitude Medium Endurance UAV similar to the Falco-EVO. The reference take-off mass is 650kg, including the mass of the conventional no-hybrid power system consisting of a Wankel engine connected to the propeller through a mechanical transmission. The typical mission of this kind of aircraft includes a take-off from the base, two climb phases with different rate of climb, and an outbound towards the reconnaissance site where the UAV performs its operation (loitering-on-site). Then, the UAV returns to the base (inbound), descends and lands. A previous analysis of the UAV with the original power systems (Donateo et al. 2016) allowed us to estimate the power request at the propeller axis in the different phases of typical flight as shown in Table 1. These values were obtained by a balance of the forces acting on the airplane and literature-derived values for the propeller efficiency. For more details, please read Donateo et al. 2016.

Table 1 Target mission of the UAV

Flight phase	Mechanical power at propeller [kW]
Take-off	63.4
Climb1	30.8
Climb2	17.2
Outbound	14.1
Loiter	10.8
Descent	11.5
Landing	9.7

Besides the general advantages described in the introduction, the usage of electrified power systems in UAVs for civil and military applications guarantees further benefits like the reduction of thermal and acoustic signature. Moreover, it is possible to improve the performance of the vehicle, like increasing service ceiling or allowing take-off from a shorter runaway (Donateo et al. 2018). Oron, 2006 listed the type of propulsion systems used in UAVs according to their installed Brake Horse Power (BPH) as reported in Table 2. Electric propulsion is preferred when the installed brake horse power

(BHP) does not exceed few kilowatts, while positive displacement engines are used between 12 and 190kW and gas turbine engines for higher power ranges.

The UAV considered in this investigation belongs to the class of UAVs for which Wankel engines are preferred (Table 2). Wankel engines are positive displacement thermal machines but, unlike reciprocating engine, the variation of volume in the thermodynamic cycle of the engine is carried out by a rotors/stator device instead of a piston/cylinder system. Wankel engines are characterized by high power density, low cross sectional area, modularity, a reduced number of parts and, above all, low levels of vibration with respect to piston engines (Meng et al. 1984, Lu et al. 2019). Moreover, they generate flat torque characteristics and have high performance at high speed. Their main drawback is the poor fuel economy due to the long combustion-chamber design. This has lead, in recent years, to a number of studies trying to improve the combustion processes in this kind of engines. An example can be found in Poojitganont et al. 2019. However, another way to improve the overall efficiency of this propulsion system could be the usage of hybridization as proposed in this investigation.

Table 2 Engines for UAVs (Oron, 2006)

UAV Type	Engine type	Power range (kW)
Mini	Two-stroke gasoline	1-15
Small tactical	Rotary engine (Wankel)	15-70
MALE (Medium Altitude Long Endurance)	Four stroke piston engines	60-190
MALE (Medium Altitude Long Endurance)	Turbo-prop	190-370
HALE (High Altitude Long Endurance)	Turbo-Jet/Fan	>370

A parallel configuration was preferred for this UAV for the higher overall efficiency and the lower number of components with respect to the series case. Figure 1 represents a scheme of the proposed parallel hybrid-electric powertrain, consisting of a Wankel engine and a permanent magnet electric machine mechanically connected to the propeller. Lithium-polymer batteries are considered here as representative of best today technology for electric storing.

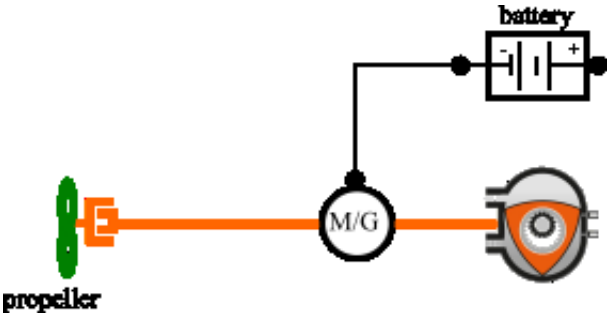

Figure 1 Parallel hybrid-electric powertrain configuration

Four operating modes are possible in a parallel power system according to the value of a power split ratio U that, at each phase of flight, defines which rate of the overall power request has to be delivered by each of the two power-flow branches, electric and thermal:

1. *Thermal*: the engine produces all the power required by the propeller (U=0);
2. *Electric*: the propeller shaft power is generated by the motor using the battery as only energy source (U=1);
3. *Charging*: the engine generates the power to move the propeller and to charge the battery while the electric machine works as a generator (U<0);
4. *Power-assist*: both the engine and the motor generate mechanical power that is delivered to the propeller (0<U<1).

Modelling the power system

Before explaining the modelling and sizing approaches, it is important to clarify the meaning of the following terms in this paper:

- "phase" defines the mission in terms of take-off, climb, cruise or loiter, descent, landing;
- "segment" refers to the discretization of the mission for the energy analysis;
- "piece" refers to a part of mission grouping adjacent segments characterized, without interruption, by the same energy mode (i.e. by the same value of U).

The mission of the UAV is discretized, for the energy analysis, as a take-off of 30s, a sequence of N_{segm} segments of 720s and a landing of 30s. In each segment, the inputs to the model are the power request at the propeller axis and value of the power-split ratio *U(isegm)* decided by the energy management strategy. The power request is based on the value of Table 1 but corrected, as explained later, according to the weight of the new powertrain and to the fuel consumption in the previous segments.

The thermal engine and the electric machine are treated as energy converters and modelled with the Willans line approach (Guzzella and Sciarretta 2007) that expresses the relation between the input and output (mechanical) power as:

$$Pout = e \cdot Pin - P_0 \tag{3}$$

where P_{in} is the chemical power in the case of engines (P_{chem}) and the electric power in the case of motors. The parameter *e* is the intrinsic "indicated" efficiency of the energy converter while P_0 accounts for the losses occurring after the energy conversion (frictions, pumping, heat losses, etc.). For permanent magnet electric machines with a nominal power close to 30kW, Guzzella et al. 2007 proposes e=0.96 and P_0=1.4kW. For thermal engines, the two parameters of the model are usually expressed as a function of engine speed, and are strongly dependent on engine technology.

The battery is treated as a reversible energy storage system and simulated with an electric circuit equivalent model, when in discharge, and with an empirical model during charging. Both models were developed and validated with experimental data on Lithium-polymer batteries in a previous investigation (Donateo et al. 2018).

Table 3 reports the main features of the models and the relative references where they are explained and validated.

Table 3 Summary of the models and references

Component	Input of the simulation block	Output of the simulation block	Modelling approach	Reference
Electric machine as motor	Mechanical power	Electrical power	Willans line efficiency model for permanent magnet machines	Guzzella et al., 2007
Electric machine as generator	Electrical power	Mechanical power	Efficiency mirrored from the behaviour as motor	Guzzella et al., 2007
Engine	Mechanical power	Chemical power (fuel flow rate)	Scalable Willans line model	
Battery (discharge)	Required power Old state of charge	Battery current New state of charge	Modified Shepherd model for lithium-polymer batteries	Donateo et al. 2018
Battery	Charge current Old state of charge	Required electric power New state of charge.	Experimentally validated empirical charging model for lithium-polymer batteries	Donateo et al. 2018

More details are needed for the model used for the Wankel engine, which was developed by the authors and introduced in this paper. In order to evaluate the benefit of hybridization for the UAV, it was necessary to develop a model of the Wankel engine that, with reasonable accuracy but low computational time, would allow us to evaluate its off-design efficiency and, therefore, to calculate the flows rate in each segment.

Moreover, hybridization can take advantage from the reduction of the engine nominal power (downsizing). Therefore, it was necessary develop a scaling procedure for the engine. The concept of scalability is meant as the possibility to obtain a good estimation of the behaviour of an energy device, starting from available data of a reference device with the same technology but different size. This aspect is crucial in the sizing of a hybrid electric power system.

In this investigation, we used the AR682 of UAV Engines LTD as reference engine because of the availability of information on this engine (in particular we had the efficiency map of the engine thanks to a personal communication with the manufacturer). The datasheets of other Wankel engines of the same manufacturer (UAV engines datasheets, 2019) were used for the validation. They are listed in Table 4.

Table 4 UAV's Wankel engines specifications from manufacturer

Engine	Number of rotors	Displacement	Power output	Mass	Nominal SFC
AR682	2	294 cc	56 kW (75 bhp) @ 6000 rpm	51.0 kg	316.3 g/kWh (0.52 lb/bhp/h)
AR682R	2	294 cc	67 kW (90 bhp) @ 7000 rpm	56.5 kg	334.6 g/kWh (0.55 lb/bhp/h)
AR741	1	208 cc	28 kW (38 bhp) @ 7800 rpm	10.7 kg	346.7 g/kWh (0.57 lb/bhp/h)
AR801R	1	294 cc	38 kW (51 bhp) @ 8000 rpm	25.4 kg	316.3 g/kWh (0.52 lb/bhp/h)

For the original configuration we considered the AR682 class that exhibits a nominal power of 56kW at 6000rpm but can reach 67kW at 7000rpm (AR682R), thus allowing the mission of Table 1 to be performed. Since the size of the engine in the hybrid systems is defined by the optimization, we developed a method to obtain the efficiency of a Wankel engine with a nominal power between 20 and 80kW together with its nominal speed, displacement, expected mass and occupied volume.

The procedure is based on the assumption that all engines belonging to the same technology (spark ignited rotary engines in this case) have similar values of brake mean effective pressure *bmep* and tangential rotor speed v_r and the same efficiency map in terms of *bmep* and v_r (Guzzella et al. 2013). Therefore, the engine brake power is proportional to its displacement while the revolutions per minutes are inversely proportional to the engine size. Note that the procedure can be applied to any kind of positive displacement engines.

As shown in the flow chart reported in Appendix (Figure A- 1) the procedure starts form a tentative value of the displacement and performs two iterations until the displacement of the engine and its rev per minutes are calculated with the selected accuracy.

For the Wankel engine, a constant power-to-weight ratio of 1 kW/kg is assumed. Therefore, the engine mass is calculated as follows.

$$Mass = Pice\_n$$

The engine volume is assumed proportional to the product of displacement and number of rotors:

$$Vol = Vol\_ref \ \frac{N\_rot \cdot disp}{N\_rot\_ref \cdot disp\_ref}$$

In these equations, *, N_rot* is the number of the engine rotors, *disp* is the displacement of a single rotor, *Pice_n* is the engine nominal power, *Vol* is the engine volume, and *Mass* is the engine mass. Subscript *"_ref"*, identifies the quantities related to the reference engine.

As shown in Figure 2, the scaling procedure allows the estimation of the engine specifications as a function of the desired nominal power with a reasonable accuracy (Table 4). Unfortunately, we had no information about the volume occupied by the UAV Ltd engines.

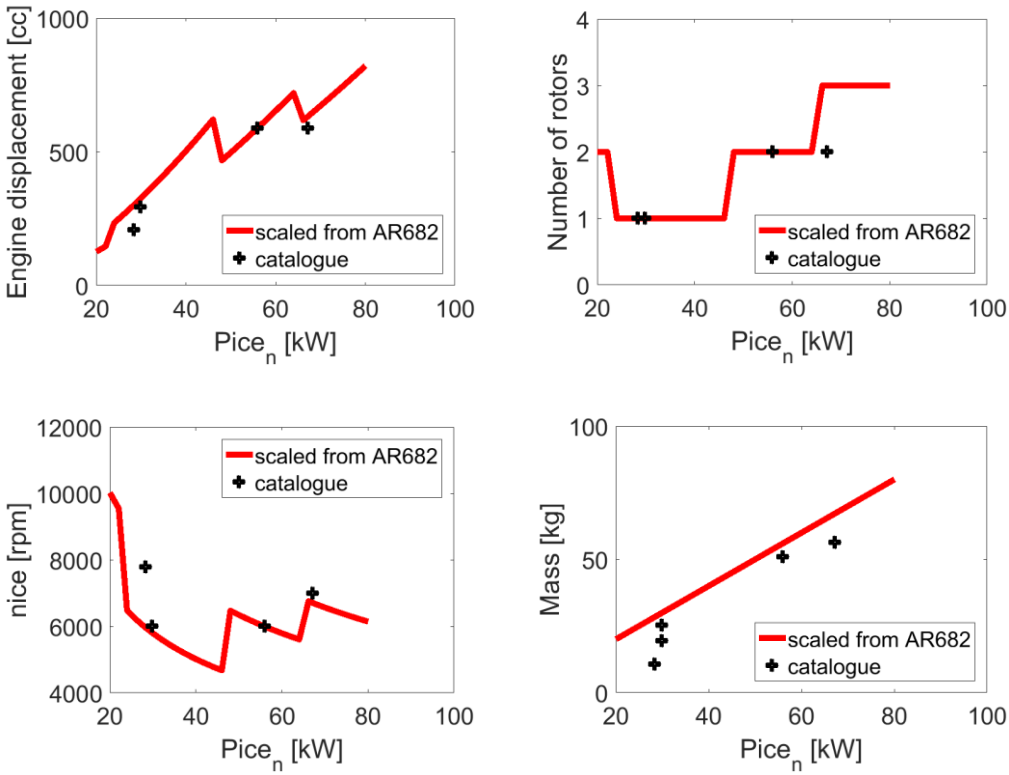

Figure 2 Validation of the scaling procedure for the Wankel engine

Once the size of the engine has been defined, the specific fuel consumption at each segment is calculated as a function of altitude and power request while the engine speed is set equal to its nominal value ($n_{ice}(isegm)=n\_ice$).

To allow the application of the model to any size in the range 20-80kW, the Willans line model is expressed in terms of brake mean effective power (bmep) and available mean effective power (amep), defined as follows:

$$bmep = \frac{P_{ice}(isegm)}{\frac{n_{ice}\ (isegm)}{60} \cdot disp} \tag{4}$$

$$amep = \frac{P_{chem}(isegm)}{\frac{n_{ice}\ (isegm)}{60} \cdot disp} = \frac{w_{fuel}(isegm) \cdot LHV}{\frac{n_{ice}\ (isegm)}{60} \cdot disp} \tag{5}$$

Where $w_{fuel}(isegm)$ is the fuel flow rate of the segment isegm and *LHV* is the lower heating value of the fuel.

The numerical coefficients of the model are obtained by fitting the SFC map that was made available by the manufacturer for the AR682 engine as explained in Figure 3:

$$bmep = e(n_{ice}) \cdot amep - p_0(n_{ice}) \tag{6}$$

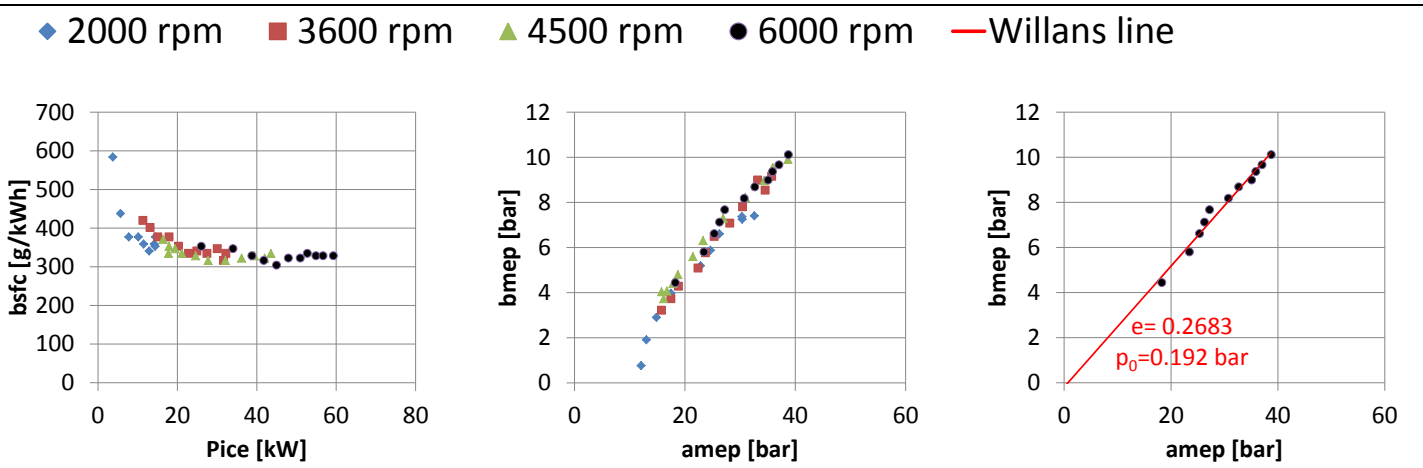

a) data of SFC versus speed and power as given by AR682 manufacturer

b) representation of the available data as scalable quantities at different engine rpm

c) Willans line as linear interpolation of available data (at 6000 rpm)

Figure 3 Fitting procedure to derive the coefficients of the Willans line at different engine speed

The performance of the engine and its efficiency at high altitude are different from sea level (SL). As known in literature, (McCormick, 1995) a "corrected density" σ can be used to decrease bmep according to the atmospheric pressure and temperature at flight level *z* :

$$\sigma(z) = \frac{p(z)}{p_{SL}} \sqrt{\frac{T_{SL}}{T(z)}} \tag{7}$$

For example, increasing the altitude from 2400m to 4200m the correct density (and so the engine power) is reduced by 80%. This is perfectly in accordance with the experimental results of Sarveswaran et al. 2003 that measured the performance of a Wankel engine in a climatic test facility. More details on the correction with altitude and on the validation of this approach can be found in Donateo et al. 2016.

Note that the effect of altitude on the power that the engine can deliver, leads to a variation of the HF during the flight, therefore, it could be reasonable to define the hybridization factor in this way:

$$HF(z) = \frac{P_{EM}}{P_{TOT}(z)} = \frac{P_{EM}}{P_{ICE}(z) + P_{EM}} \tag{8}$$

The design approach

The methodology proposed by the authors is the combination of the simulation approach described in the previous section with multi- and many-objective genetic algorithms (suitable for problems with more than one optimization goal and more than 3 goals, respectively).

The ultimate goal of the design is to keep the take-off mass, and therefore the power request of the hybrid configuration, as close as possible to the baseline conventional case and to improve, if possible, fuel economy and payload by acting on the sizing (power and energy hybridization factors) and on the energy management (power split factor U). In the approach proposed here, the design and the energy management are optimized in a single optimization run and the final value of the battery state of charge (SOC) is left unconstrained.

From a mathematical point of a view, we formulated a two-objective optimization problem where the goals are the overall fuel consumed in the reference mission (M_{fuel}), to be minimized, and the maximum payload weight (W_{pay}) to be maximized. Note that the payload and M_{fuel} are competitive metrics because the reduction of fuel consumption is possible if larger batteries are used. On the other hand, increasing the mass of the battery, the payload is reduced. This will be more evident in the analysis of the results.

The input variables are the power split factor U in each segment of the mission, the energy stored in the battery (individual battery capacity C_{cell} and number of battery packs in parallel $n_{p,bat}$) and the charging rate of the battery (c_{rech}). In formulas:

$$\bar{x} = \left[U;\ C_{cell};\ n_{p,bat};\ c_{rech}\right] \text{ with } U = \left[U\left(i_{segm}\right)\right],\ i = 1, \dots, N_{segm} \tag{9}$$

$$U\left(i_{segm}\right) = \frac{P_{EM(i_{segm})}}{P_{TOT}\left(i_{segm}\right)} = \frac{P_{EM}\left(i_{segm}\right)}{P_{ICE}\left(i_{segm}\right) + P_{EM}\left(i_{segm}\right)} \tag{10}$$

The ranges of variation of the input variables are shown in Table 5. The size of battery, engine and motor (and the corresponding values of the hybridization factors) are intermediate results of the optimization.

Table 5 Input variables of the optimization

Variable	Lower / Upper limits	Notes
U (i_{segm}) for each i_{segm}=1:N_{segm}	-0.01 / 1	-0.01=CHARGING 0 THERMAL 1 ELECTRIC (0,1) POWER-ASSIST
C_{cell} [Ah]	11 / 53	Individual battery cell capacity
$n_{p,bat}$	1 / 15	Number of battery cells in parallel
c_{rech}	0.1 / 3	Charging rate

Constraints about MTOW and the volume are included in the optimization to allow the new powertrain to be used without modification to the original UAV architecture. Furthermore, a constraint on the engine power is due to the necessity of remaining in the size range of Wankel engines

$$MTOW_{hybrid} = MTOW_{baseline}$$
$$Vol_{hybrid} \leq Vol_{baseline} \tag{11}$$
$$20\ kW \leq P_{engine,nom} \leq 80\ kW$$

Where $MTOW_{hybrid}$ and $MTOW_{baseline}$ stand for the Maximum Take-Off Weight of the hybrid and baseline configurations, respectively, while Vol_{hybrid} and $Vol_{baseline}$ are the power system volume for the two architectures, $P_{engine,nom}$ is the nominal power of the engine in the hybrid system. Note that the reference values are $MTOW_{baseline}$, 650 kg, $Vol_{baseline\ f} \cong 0.257\ m^3$, (including engine and additional fuel tanks under the wings).

According to the values of the input parameters defined by the optimization algorithm, an in-house code carries out the sizing of each component of the hybrid-electric power system by performing a series of steps that are described below and illustrated as flowcharts in the Appendix.

STEP 1: Applying the power-split

At each segment, the mechanical power request is split between the electric and thermal lines as a function of the corresponding value of $U(i_{segm})$;

$$P_{ice}(i_{segm}) = \left[1 - U(i_{segm})\right] \cdot P_{ax,prop}(i_{segm})$$
$$P_{mot}(i_{Segm}) = U(i_{segm}) \cdot P_{ax,prop}(i_{segm}) \tag{12}$$
$$P_{bat}(i_{segm}) = \frac{P_{mot}}{{\eta_{mot}}^{\gamma}}$$

where $P_{ice}(i_{segm})$, $P_{mot}(i_{segm})$, and $P_{bat}(i_{segm})$ are the power of internal combustion engine (ICE), motor, and battery, respectively, at the mission segment i_{segm} while, $P_{ax,prop}(i_{segm})$ is the mechanical power required at the propeller axis. Note that γ is used to identify if the electric machine in working in motor mode ($\gamma = 1$) or used as a generator ($\gamma = -1$).

STEP 2: Sizing the electric machine

The electric machine is sized according to the maximum absolute value of P_{mot} over the whole mission. The volume (V_{mot}) and mass (M_{mot}) of the motor are calculated as in Eqs. (13):

$$M_{mot} = \frac{C_{bat}}{0.0482 \cdot C_{bat} + 1.288} + 0.339 \cdot P_{mot,n} + 5.45$$
$$V_{mot} = (Vm_0 + C_{bat} \cdot Vm_1) + 0.57 \cdot P_{mot,n} + 7.94 \tag{13}$$

where Vm_0, Vm_1, and the constant values are statistically derived parameters (Donateo et al., 2018) while, $P_{mot,n}$ is the nominal motor power, and C_{bat} is the battery capacity $C_{bat} = C_{cell} \cdot n_{p,bat}$.

STEP 3: Sizing the battery

As are result of the previous step, the procedure separates the mission pieces characterized by DISCHARGE or CHARGING mode for the battery, and calculates the array $P_{bat,vect}$ which contains the battery power of each segment belonging to the mission piece "j". The battery model is used to calculate the corresponding values of voltage and current of the battery $I_{bat,vect}$. Then, the battery sizing procedure increases the number of battery cells in series until it is possible to perform the whole mission without discharging the battery under 20% of the nominal capacity and without exceeding the acceptable discharging and charging rates (that are chosen according to the Kokam's database for lithium-polymer batteries). The procedure is iterative because the state of charge of the battery at the beginning of each piece is the results of the analysis of the power request of the previous piece and of the battery size (see Figure A- 2 and Figure A- 3).

STEP 4: Sizing the engine

The Wankel engine is sized according to its maximum power request over all segments. In the mission pieces with battery in charging, the engine power is the sum of the required propulsive power and the power to charge the battery.
The maximum power request of the engine is corrected to take into account the loss of power with altitude. Therefore, the actual engine size is defined according to the power at sea level:

$$P_{ice,SL} = P_{ice} \frac{p_{SL}}{p_0} \sqrt{\frac{T_0}{T_{SL}}} \tag{14}$$

where the subscripts "SL" and "0" refer to the sea-level and high altitude conditions, respectively.
The engine mass (M_{ice}) and volume (V_{ice}) are then calculated with the Wankel downsizing procedure.

STEP 5: Recalculating the power request

The weight of the aircraft during the mission decreases due to fuel consumption. Therefore, the power at propeller axis at each mission segment in the hybrid-electric configuration could be different from the values of Table 1(which refer to the baseline power system) because of the different fuel consumption. This was taken into account in this investigation by upgrading the power request of each segment according to the fuel consumption in the previous time steps.

STEP 6: Calculating the fuel consumption

From the engine size and its operating points it is possible to calculate the amount of fuel consumed during each flight segment and the total mass of fuel required for the mission (M_{fuel}), by using the Willans Line model applied to the Wankel engine.

STEP 7: Calculating payload

The payload mass M_{pay} is estimate as:

$$\mathrm{M_{pay}} = \mathrm{M_{takeoff}} - M_{fuel} - M_{batt} - M_{ICE} - M_{mot} - M_{empty} \quad (15)$$

with M_{empty} equal to 400kg (the same of the baseline architecture).

STEP 8: Feasibility analysis

If W_{pay} is negative, the solution is considered unfeasible in the optimization. Similarly, the solution is unfeasible if the other constraints are not satisfied.

Results and discussion

The optimization algorithm used in this investigation is the S-Metric Selection Evolutionary Multi-Objective Algorithm (SMS-EMOA) (Emmerich et al., 2005) that was found particularly valuable in addressing the topic of aircraft electrification (see Donateo et al. 2019). The optimization was performed with a population of 450 individuals that evolved along 100 generations, resulting in 45000 design evaluated during the whole process. The whole process is summarized in the flowchart of Appendix A (Figure A- 4).

Figure 4 shows the values of the objective functions for the 40 optimal solutions (Pareto front) compared with the fuel consumption and payload of the original baseline configuration (calculated with the model proposed here for the Wankel engine AR682): M_{fuel}=86.4kg and M_{pay}=100.2kg. To better put into evidence the (limited) improvements obtained with the optimization with respect to the baseline case, the goals are expressed in terms of saved fuel and added payload. The size of the bubbles represents the energy stored in the battery that ranges, in the Pareto front, between 3 and 6kWh while a colour bar is used to underline the power hybridization factor HF of each solution.

Reading the Pareto front from the right (saved fuel) to the left (increased payload), we confirm the competitiveness of the two optimization goals and notice a general trend in HE (battery size) and HF, with few exceptions. In particular, the increase of payload at the expenses of consumed fuel is obtained by increasing the power hybridization factor and reducing the energy hybridization factor (smaller size of the battery). Note that there are some discontinuities in the Pareto front due to the procedure used for the sizing of the battery. As already explained, the battery is chosen from a commercial database, therefore, the values of energy density and charging rate are not the same for all batteries. This also could explain the exceptions to the general trends highlighted above.

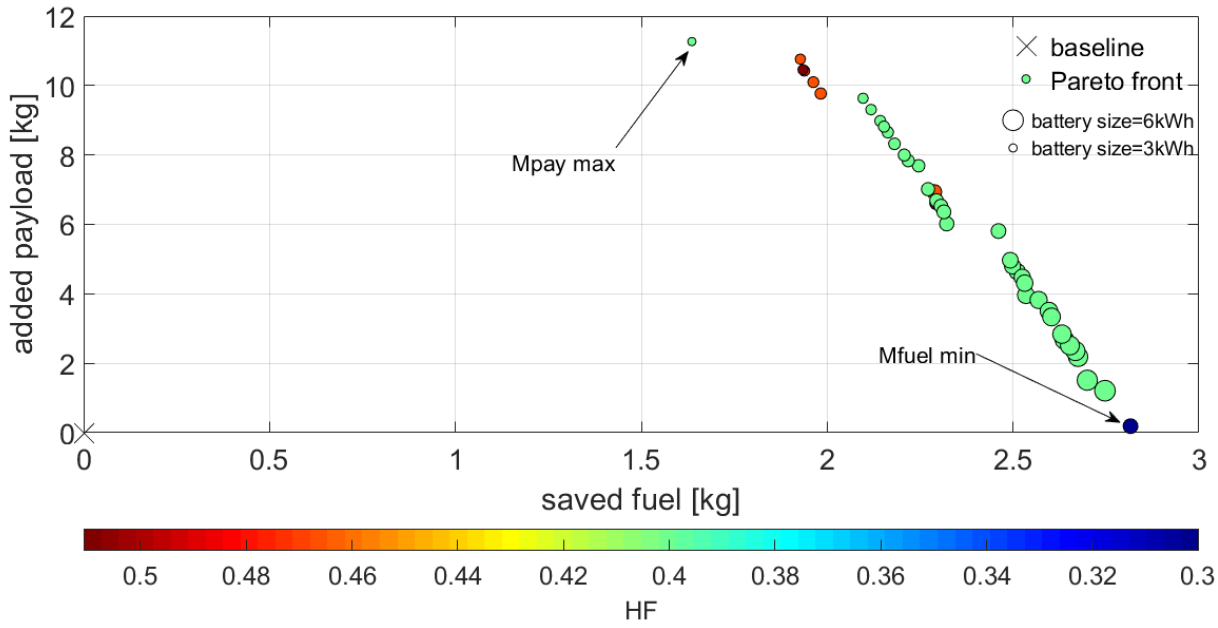

Figure 4 Results of the optimization in terms of added payload, saved fuel, battery size and power hybridization factor

The solutions of the Pareto front represent different levels of compromise between the two goals and the choice of the particular solution is left to the decision maker. In this work, we will analyse the two “edge solutions” denoted in Figure 4 as “Mfuel min” and “Mpay max”.

“Mfuel min” guarantees a 3.24% reduction of the overall fuel consumption with respect to the baseline value and about the same maximum-payload mass (+0.2%). The percentage of fuel saving of 3% is in line with what found by Frosina et al. in (Frosina et al., 2018). “Mpay max” gives a 11% more payload than the original case but with a lower fuel saving (1.8%).

Figure 5 shows the weight distribution of the different contribution in the optimal hybrid electric power systems. Note that the additional mass of battery and motor is balanced by the combined effects of a lighter engine and a better fuel economy of the hybrid configurations. In fact, the engine is strongly downsized with respect to the original configuration in both cases (44kW for “Mfuel min” and 38kW for “Mpay max”). Note that the engine nominal power of the “Mpay max” solution corresponds to the engine model AR801R of Table 4. The predicted mass of the engine (38kg) is actually lower than the value declared by the manufacturer (25.4kg), thus accommodating inaccuracies in the estimation of the other weights (battery, motor and other electric components).

Since the take-off weight is the same for all cases and the fuel consumption in the different phases of the mission is pretty much the same, the correction applied by the method to the power request of Table 1 for the hybrid cases was totally negligible.

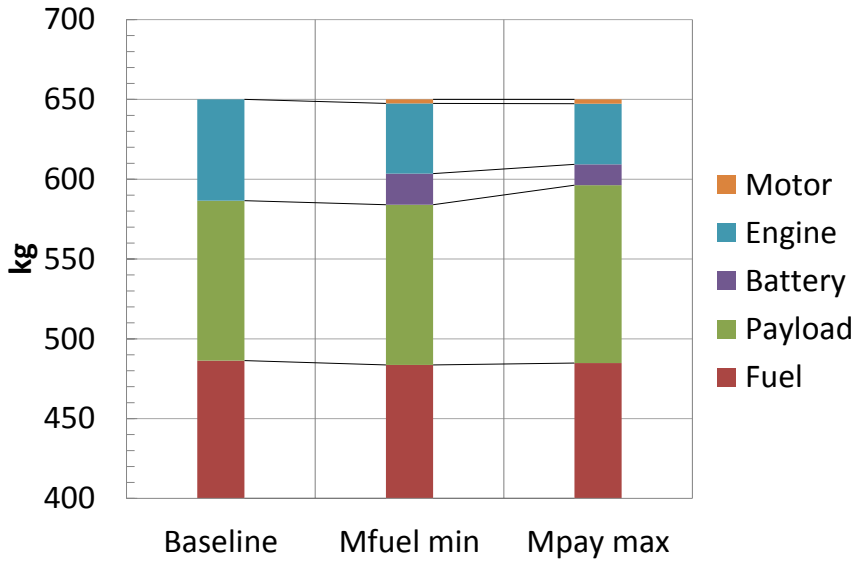

Figure 5 Weight distribution of the optimal hybrid configurations compared with the baseline case

As for the battery, the same reference cell is used in “Mfuel min” and “Mpay max”. The different performances of the two configurations are the results of a different combination in series and in parallel (see Table 6).

Table 6 Battery specification for the optimal solution from Kokam's database (2019)

	Mfuel min	**Mpay max**
Cell model	SLPB065070180	SLPB065070180
Gravimetric energy density	246.0 Wh/kg	246.0 Wh/kg
Volumetric energy density	418.5 Wh/l	418.5 Wh/l
Maximum (continuous) rate of discharge	2C	2C
Cell capacity	11.6 Ah	11.6 Ah
Vbus	414.4V	140.6V
String in parallel	1	2
Battery energy	4.8kWh	3.2kWh

The plots of Figure 6 show how the battery is used along the mission in the selected solutions, disclosing only small differences between the two cases. In both cases, in fact, the battery helps the engine at take-off with a value of the power split U equal to the hybridization factor of the configuration. Then, the battery is used no more (with few exceptions) in the climb and loiter phases. The reason is that using the thermal mode at constant flight conditions produces a fast consumption of fuel that reduces the weight of the aircraft and therefore, the power request. A small portion of the descent is performed in electric mode (in “Mfuel min”) or with a large U (in “Mpay max”) and this rapidly decreases the battery

state of the charge. The low power request during descent allows the engine to charge the battery. Finally, the battery is used again in power assist mode at landing.

The final state of the charge of the battery (SOC) is similar for the two cases (23% for “Mfuel min” and 25% for “Mpay max”).

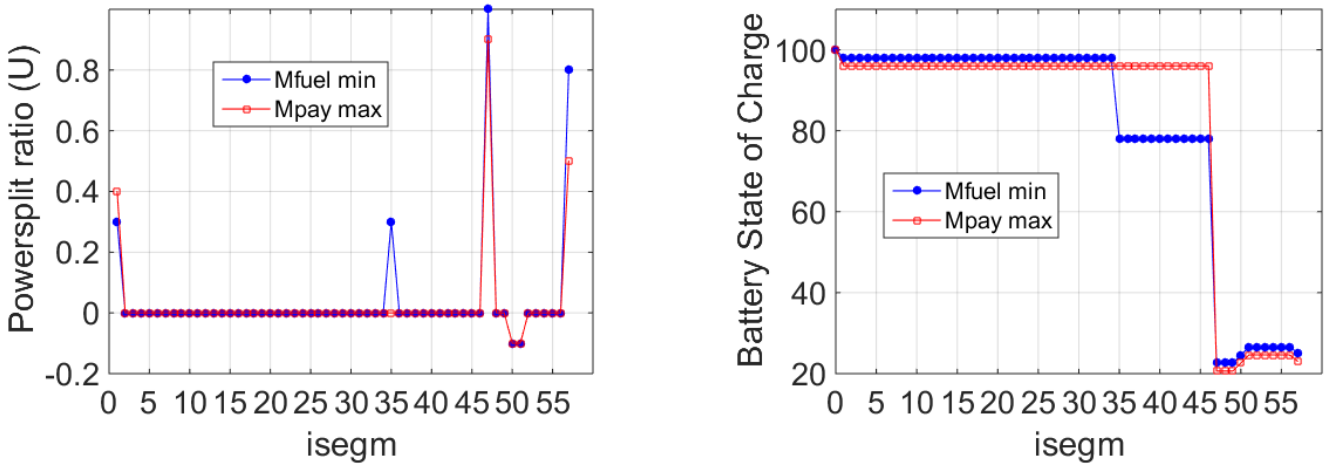

Figure 6 Usage of the battery along the mission for the two solutions (“Mfuel min” and “Mpay max”)

From the results shown above, it is evident that the fuel reduction with respect to the baseline case is possible thanks to different effects. The first one is the downsizing of the engine due to the contribution of the battery to the take-off power. This makes the engine working closer to its nominal power during the other mission segments characterized by much lower power request than the take-off phase. In turn, this allows a reduction of the specific fuel consumption in those segments and, therefore, improves fuel economy. However, the most important contribution to fuel saving, in both cases, is that part of the energy required by the mission is given by the battery that is almost fully discharged from take-off to landing. For this reason, the fuel saving increases with the energy hybridization factor. Since the two forms of consumption (fuel and electricity) cannot be summed, one could convert them into either CO_2 emissions or costs per mission. In this way, it is possible to put better into evidence the environmental and money-saving advantages of hybridization.

Benefits in terms of environment and costs

The emissions of carbon dioxide of any vehicle can be divided into direct and indirect contributions.

The direct or local emissions are those from the engine burned during the flight and are directly proportional to fuel flow rate. If we consider an emission factor of 8.31 $kgCO_2/gal$ for the aviation gasoline "AvGas" (Emission Factors for Greenhouse Gas Inventories, 2014), we obtain:

$$Local\ emissions\ = M_{fuel} \cdot 8.31 \cdot 0.227 \tag{16}$$

where 0.227 is the conversion factor from gallon to kilogram.

Indirect or "well-to-tank" emissions are related to the process of obtaining the energy stored in the aircraft and used for the flight. For the gasoline, the well-to-tank emissions associated to production and distribution are estimated to be 17% of direct emissions while 0.3985 kg/kWh is the CO_2 emission factor of electricity production in Italy (Brander et al. 2019).

Therefore, one can calculate the total emissions as:

$$Total\ emissions\ 1.17 \cdot Local\ emissions + 0.3985\ \cdot kWh \tag{17}$$

where kWh is the amount of electricity consumed in the mission that can be estimated as:

$$kWh = \mathrm{E_{batt}} \cdot (SOC_{in} - SOC_{fin})/100 \tag{18}$$

where SOC_{in} and SOC_{fin} are the initial and final state of the charge of the battery in the mission.

For the "Mfuel min" case, we obtain 186 kg vs 190.7 kg of the baseline powertrain (-2.5% for total emissions).

The costs for fuel and electricity are estimated as follows:

$$Baseline\ cost = M_{fuel} \cdot 6.2 \cdot 0.227$$

$$Hybrid\ cost = M_{fuel} \cdot 6.2 \cdot 0.227 + 0.23 \cdot \mathrm{kWh}$$

where 6.2 USD/gallon is an average value of the specific cost of the AvGas in 2015 (Jet-A and Avgas Fuel Prices: August 2015), 0.227 is the conversion factor from gallon to kilogram, and 0.23 USD/kWh is the electricity specific cost in Italy (Electricity prices, 2019). Overall, we obtain a reduction by 3% in the cost per mission for the "Mfuel min" case (from 121.6 USD of the baseline case to 117.9 USD).

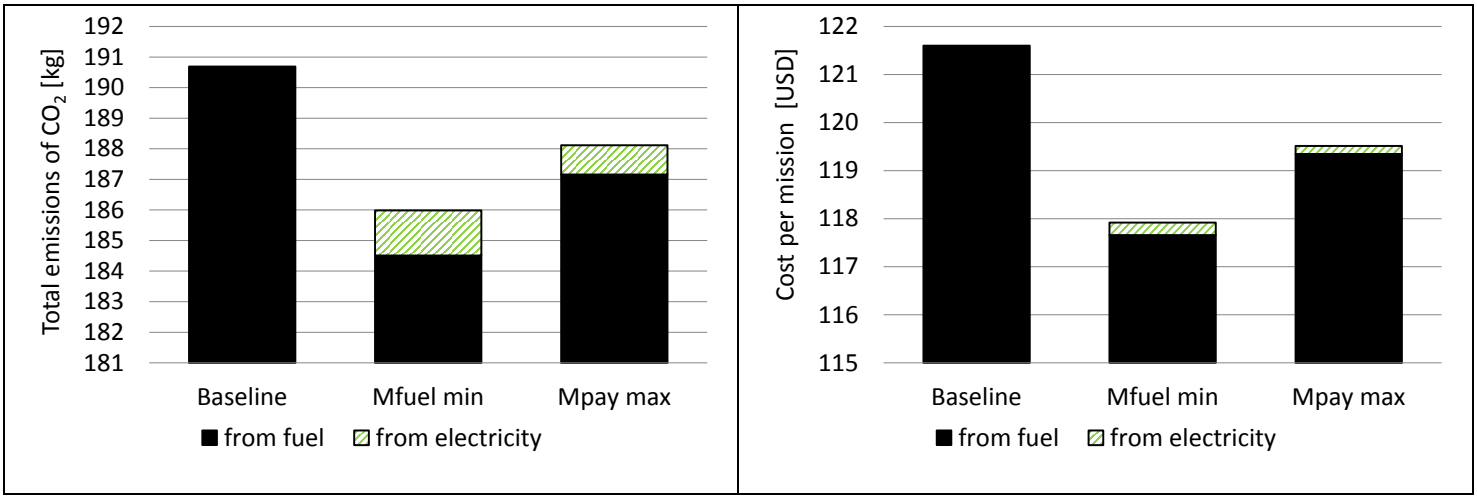

Figure 7 Advantages of the proposed hybridization solutions in terms of total emissions of CO_2 and cost per mission

The results of these analyses (Figure 7) show how the contribution of electricity is negligible both in terms of environmental impact and from the cost per mission point of view.

Benefits in terms of endurance

The optimization performed here was aimed at improving fuel economy and payload, being the mission the same. However, considering the specific application (UAV), the designer could use the saved fuel to increase the endurance i.e. the length of the mission. To consider this case, we added additional segments performed in thermal mode to the loiter phase until the total fuel per mission was equal to the baseline case. In this way, we obtained an improvement by about 4.3% in the duration of the loiter (t_{loiter} from 8 to 8.34 h) for the "Mfuel min" solution (with a penalty on payload that decreases to 97% of the baseline case). In the case of the "Mpay max" solution, we could convert the added payload in additional fuel to increase the endurance in loiter up to 9.4h (+17%) with the same payload of the original UAV.

Expected improvements in batteries

The limited improvement in fuel economy and payload are due to the unsatisfactory energy density of the batteries considered in this investigation (250Wh/kg). When better technologies for electricity storage will be available, the same optimal solution ("Mfuel min") will guarantee larger values of payload and endurance. Figure 8 shows the expected improvement of payload and endurance estimated for battery energy densities up to 750Wh/kg (Del Rosario et al. 2014). These improvements were obtained by converting the saved weight of the battery into payload or loiter time, respectively.

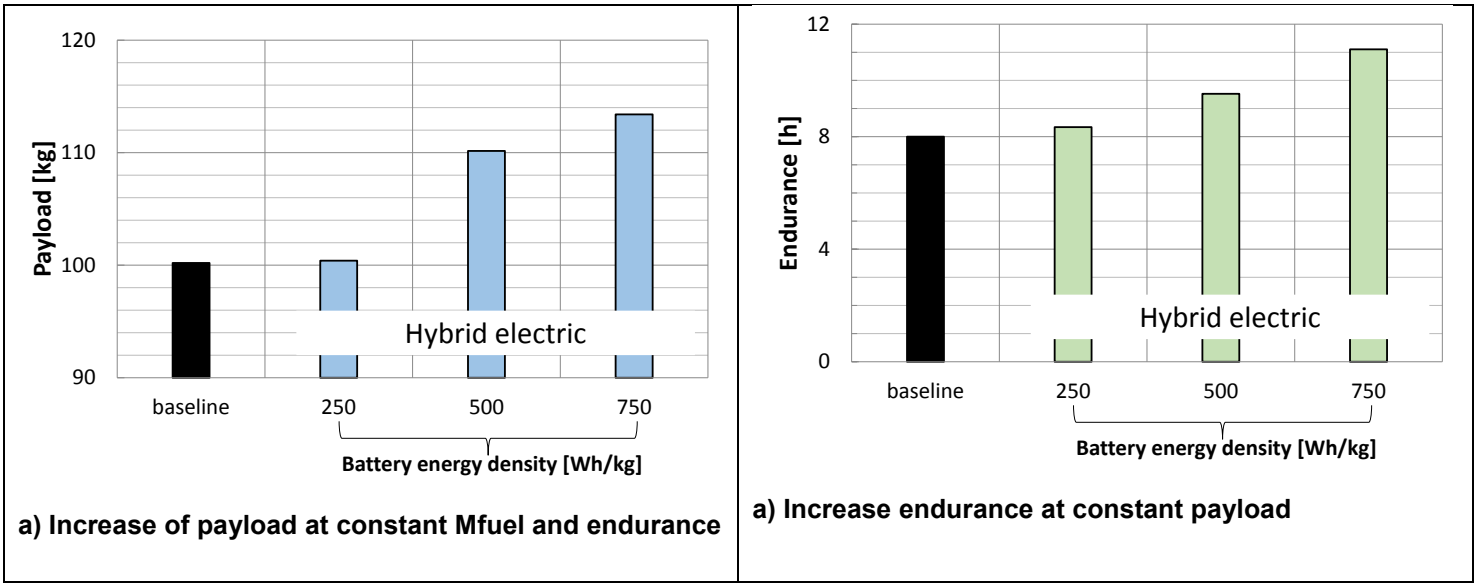

a) Increase of payload at constant Mfuel and endurance

a) Increase endurance at constant payload

Figure 8 Expected improvement of payload or endurance with technology battery developments ("Mfuel min")

Final considerations and future developments

To check whether the results were affected by the arbitrary choice of the mission, the optimization was repeated with a new power request for the baseline case, as shown in Table 7. For this mission, the baseline case presents a fuel consumption and a payload equal to 100.5kg and 86kg, respectively.

Table 7 Second mission considered for the optimization

Flight phase	Mechanical power at propeller [kW]
Take-off	52.7
Climb1	30.3
Climb2	20.5
Outbound	22.3
Loiter	10.3
Descent	7.28
Landing	5.97

The results are reported in Figure 9 with the same notation of Figure 4. Note that, even if the values of the M_{fuel} and M_{pay} are different, the general trends of the four variables displayed in the figures are the same.

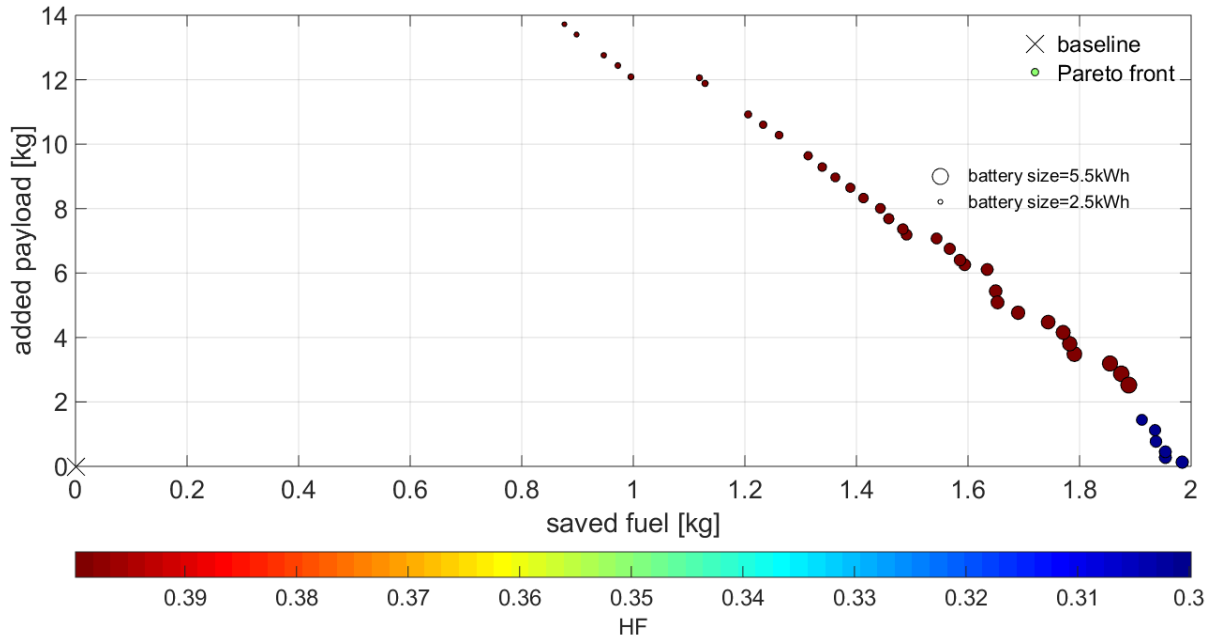

Figure 9 Results of the optimization in terms of added payload, saved fuel, battery size and power hybridization factor for the second mission

The design approach used in this work is meant to be applied during the preliminary design of the hybrid electric power system and is based on one or few typical missions of the UAV. If the UAV is called to perform other missions, it is possible to refine the energy management with off-line or on-line optimizations. To this scope, the application of the Equivalent Consumption Minimization Strategy (Guzzella et al. 2007) will be considered as further investigation. Moreover, since the contribution of electricity to CO_2 emissions and cost per mission is negligible, one could force the battery to be fully discharged at the end of the flight.

Conclusions

In this study, a design methodology for hybrid electric power systems is proposed and applied to a tactical unmanned aerial vehicle (UAV). It optimizes the power and energy hybridization factors and on the energy management strategy in order to minimize the overall fuel consumption throughout the mission (Mfuel) and maximize the aircraft payload mass (Mpay) by means of advanced genetic algorithms. The energy strategy is expressed in terms of a so-called power-split ratio (U), which defines how the mechanical power request of the propeller is satisfied by the thermal and electrical branches in each phase of the mission which is discretised in 55 segments of 720 seconds plus take-off and landing.

The size of battery, motor and engine are defined during the optimization process. The investigation also proposes a low fidelity model for design and off design analysis of Wankel engines for the specific application to tactical UAVs. However, the methodology can be applied to any kind of engines.

In this investigation, the optimization was performed over a pre-fixed mission with strong constraints on the take-off mass of the UAV and the total volume of the power system. Two solutions corresponding, on the Pareto front of the optimization, to the minimum fuel ("Mfuel min") and to the maximum payload ("Mpay max") were analysed in details. The analysis explained that, if the preference of the designer is given to fuel economy, it is necessary to use a small hybridization factor and a medium size of the battery. On the contrary, a higher hybridization factor (0.4), combined with a smaller battery, allows the payload to be increased. This statement was confirmed by repeating the optimization over a second mission.

The "Mfuel min" solution allows a 3.24 % saving of the fuel mass burned throughout the mission (or, alternative an improvement of endurance by 4.3%) with respect to the same mission executed with baseline powertrain, and about the same maximum-payload mass. The fuel economy of "Mfuel min" solution was expressed in terms of environmental and economic advantages, giving a 2.5% reduction in emissions of CO_2 (direct and indirect) and a 3% cutback of the cost-per-mission. These limited improvements are affected by the constraint related to the take-off mass and could be considered below the accuracy of the low fidelity models used for the analysis, but we are confident abut the results because the engine weight was overestimated by our method . Moreover, the goal of this investigation was to show how the proposed design methodology can be very useful to exploit today technology for engines, motors and batteries at their best, not to accurately quantify the fuel consumption. Finally, the results of the investigation showed that, considering future batteries with an energy density of 750Wh/kg, endurance could be increased by 40% by storing more fuel on the aircraft with the same payload.

References

Brander M. Sood A., Wylie C., Haughton A., Lovell J., "Electricity-specific emission factors for grid electricity", Ecometrica, https://ecometrica.com/assets/Electricity-specific-emission-factors-for-grid-electricity.pdf (accessed 06 June 2019)

Brelje, B.J., Martins, J. R.R.A., (2019) "Electric, Hybrid, and turboelectric fixed-win aircraft: A review of concepts, models and design approaches", Progress in Aerospace Sciences, vol. 104, pp 1-19.

Del Rosario, R., (2014) "A Future with Hybrid Electric Propulsion Systems: A NASA Perspective", Turbine Engine Technology Symposium, 8-11 September 2014, Dayton, OH, United States [Online]. Available https://ntrs.nasa.gov/archive/nasa/casi.ntrs.nasa.gov/20150000748.pdf.

Del Rosario, R., A Future with Hybrid Electric Propulsion Systems: A NASA Perspective, Turbine Engine Technology Symposium; 8-11 Sep. 2014; Dayton, OH; United States [Online]. Available https://ntrs.nasa.gov/archive/nasa/casi.ntrs.nasa.gov/20150000748.pdf.

Donateo, T., De Pascalis, C.L., Ficarella, (2019) "A. Synergy Effects in Electric and Hybrid Electric Aircraft", Aerospace 2019, 6, 32.

Donateo, T., Ficarella, A., Spedicato, L., (2016) "Development and validation of a software tool for complex aircraft powertrains", Advances in Engineering Software, 96, pp. 1-13. ISSN: 09659978 DOI: 10.1016/j.advengsoft.2016.01.001.

Donateo, T., Ficarella, A., Spedicato, L., (2018) "A method to analyze and optimize hybrid electric architectures applied to unmanned aerial vehicles", Aircraft Engineering and Aerospace Technology, Vol. 90 Issue: 5, pp.828-842, https://doi.org/10.1108/AEAT-11-2016-0202T.

Donateo, T., Spedicato, L. (2017) “Fuel economy of hybrid electric flight”, Appl. Energy, 206, 723–738.

Electricity prices, https://www.globalpetrolprices.com/electricity_prices/ (accessed 06 June 2019)

Emission Factors for Greenhouse Gas Inventories, https://www.epa.gov/sites/production/files/2015-07/documents/emission-factors_2014.pdf (accessed 06 June 2019)

Emmerich, M., Beume, N., Naujoks, B., (2005) “An EMO Algorithm Using the Hypervolume Measure as Selection Criterion”, in Proceedings of the Third International Conference of Evolutionary Multi-Criterion Optimization EMO 2005, Guanajuato, Mexico, 9–11 March 2005.

Fletcher, S., Flynn, M.C., Jones, C.E. and Norman, P.J., (2016) “Hybrid electric aircraft: State of the art and key electrical system challenges”, IEEE Transportation Electrification eNewsletter, September 2016.

Frosina, E.; Senatore, A.; Palumbo, L.; Di Lorenzo, G.; Pascarella, C. Development of a Lumped Parameter

Guzzella, L., Sciarretta, A., (2007) “Vehicle Propulsion Systems: Introduction to Modeling and Optimization” Springer, Berlin, Germany.

Harmon F.H., Frank A. A., Joshi S. S., “Application of a CMAC Neural Network to the Control of a Parallel Hybrid-Electric Propulsion System for a Small Unmanned Aerial Vehicle”, Proceedings of International Joint Conference on Neural Networks, Montreal, Canada. July 31 - August 4, 2005.

ICAO, Document 9963 (2010), “Report of the Independent Experts on the Medium and Long Term Goals for Aviation Fuel Burn Reduction from Technology”, Montreal.

Jet-A and Avgas Fuel Prices: August 2015, https://aviationweek.com/bca/jet-and-avgas-fuel-prices-august-2015 (accessed 06 June 2019)

Kokam Li-ion Cell database, http://kokam.com/cell/ (accessed 15 May 2019)

Lu Y., an J., Fan B., Otchere P., Chen W., Cheng B., (2019), “Research on the application of aviation kerosene in a direct injection rotary engine-Part 1: Fundamental spray characteristics and optimized injection strategies”, Energy Conversion and Management Volume 195, 1 September 2019, Pages 519-532

McCormick B. W., (1995) “Aerodynamics, Aeronautics and Flight Mechanics”, John Wiley, 1995.

Meng P, Hady W and Barrows R 1984 An overview of the NASA rotary engine research program NASA Tech. Memo. 83699 (Washington D.C.: National Aeronautics and Space Administration)

Model for an Aeronautic Hybrid Electric Propulsion System. Aerospace 2018, 5, 105.

Moore, M.D., Fredericks B., (2014) “Misconceptions of electric propulsion aircraft and their emergent aviation markets”, AIAA 2014-0535, Session: Aircraft Design with Electric Propulsion, 10 January 2014.

Oron H., (2006) “UAV Engines in the next decade – Turbine Engines, Piston Engines and the newly Combat Proven Rotary Engine”, A lecture at the 6th Symposium on Jet Engines and Gas Turbines, Haifa, 16 November 2006.

Poojitganont T, Sinchai J, Watjatrakul B.,Berg HP., “Numerical Investigation of In-chamber Flow inside a Wankel Rotary Engine” 2019 IOP Conf. Ser.: Mater. Sci. Eng. 501 012043, (2019).

Pornet C., Isikveren A.T., (2015) “Conceptual design of hybrid-electric transport aircraft”, Progress in Aerospace Sciences, 79, pp 114-135, DOI: http://dx.doi.org/10.1016/j.paerosci.2015.09.002.

Sarveswaran, V., Murthy (IN), Y., Ganesan, V., (2003) "Altitude Performance Comparison of A Wankel Engine With Carburetor and Fuel Injection," SAE Technical Paper 2003-28-0017, 2003, doi:10.4271/2003-28-0017.

Serrao L. (2009) “A comparative analysis of energy management strategies for hybrid electric vehicles”, Ph.D. Thesis, The Ohio State University.

Silvas E., Hofman R., Murgovsk N., Etman P., Steinbuch M. (2016), “Review of Optimization Strategies for System-Level Design in Hybrid Electric Vehicles”, IEEE Transactions on Vehicular Technology, pp 1-15.

Traub L. W. (2011), “Range and Endurance Estimates for Battery-Powered Aircraft”, Journal of Aircraft, Vol. 48, No. 2.

UAV engines datasheets, https://uavenginesltd.co.uk/products/ar682-75-bhp/ (accessed 05 June 2019)

Appendix A. Flowcharts of the proposed design method

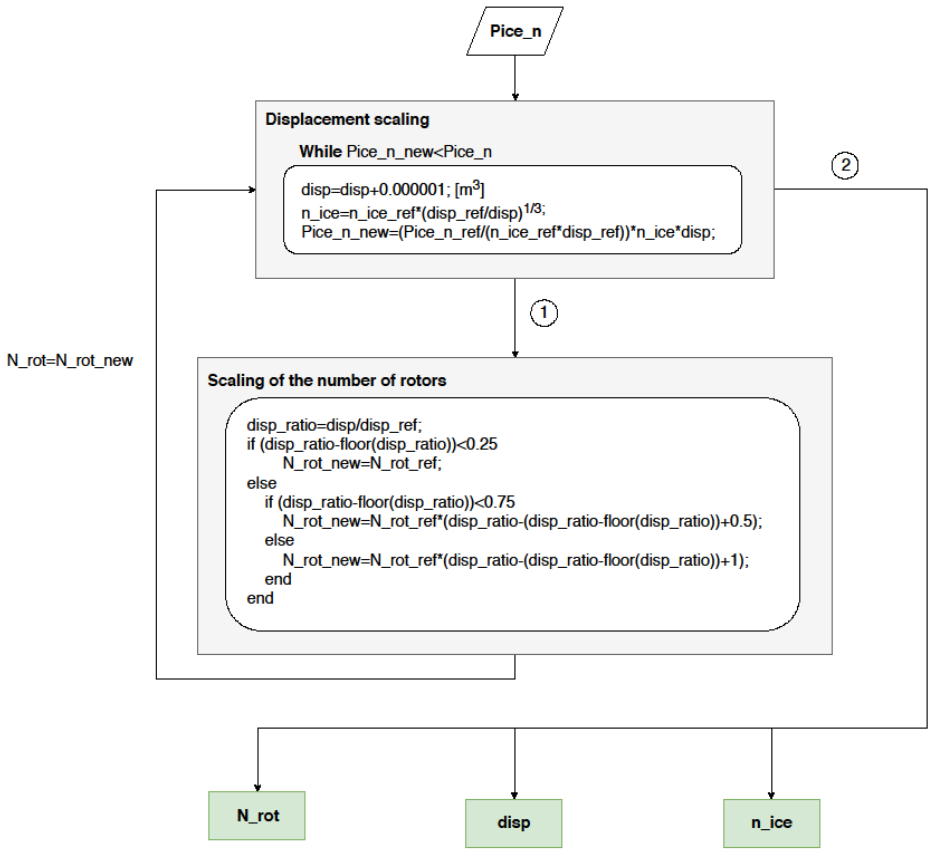

Figure A- 1: Flowchart of the Wankel engine scaling method

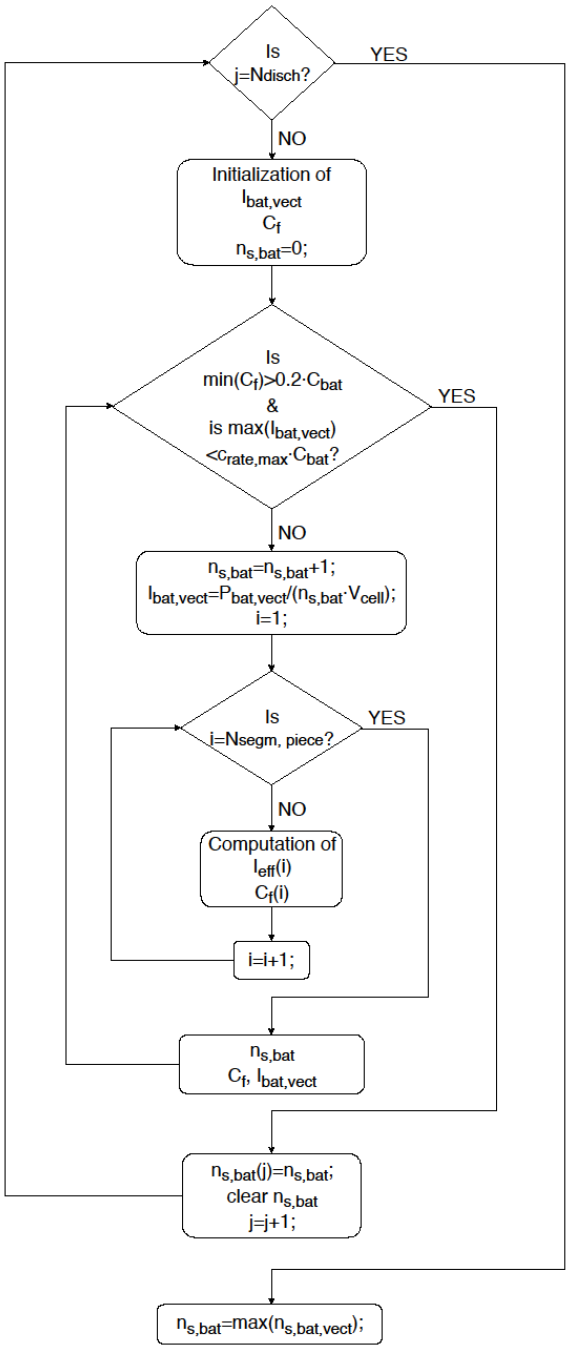

Figure A- 2: Flow chart of the battery sizing procedure

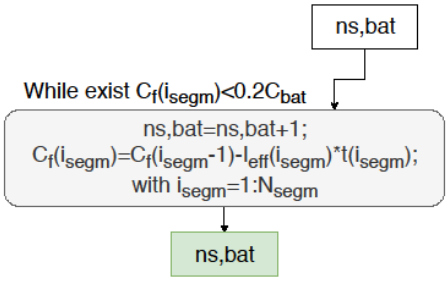

Figure A- 3: Battery size refining

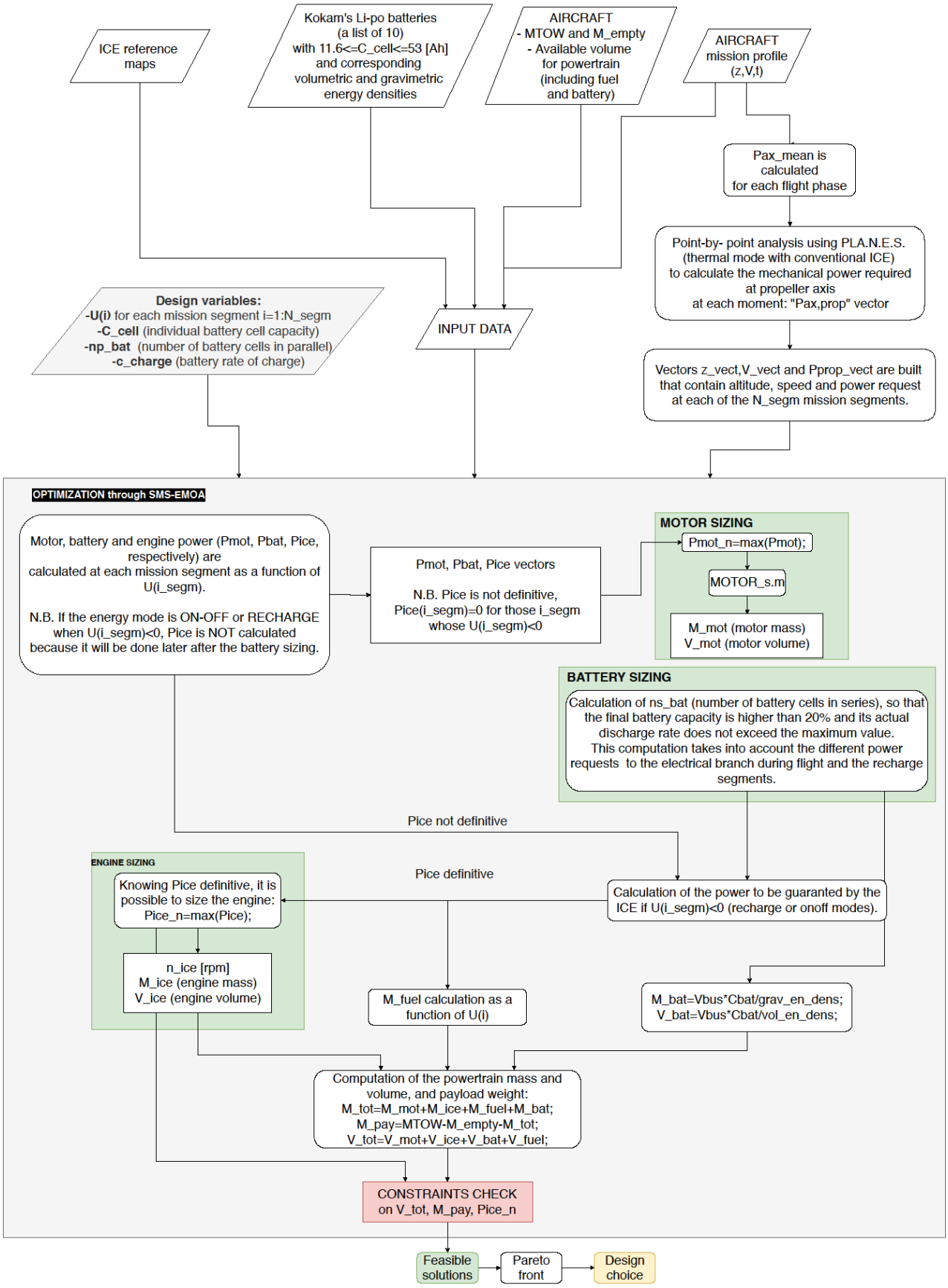

Figure A- 4: Flowchart of the overall design process

List of variables (flowcharts)

C_cell	battery cell capacity
c_charge	battery rate of charge
Cbat	battery capacity
C_{bat}	battery nominal capacity
C_f	battery capacity at the end of each segment of the mission piece
c_{rate_max}	battery maximum discharge rate
grav_en_dens	battery gravimetric energy density
i_segm	index for mission segment
I_{bat}	battery current
I_{eff}	effective battery current taking into account the Peukert's effect (Guzzella et a. 2007)
M_bat	battery mass
M_ice	engine mass
M_mot	motor mass
M_pay	payload mass
M_tot	powertrain overall mass
n_ice	engine nominal speed
N_segm	number of segments in which the mission was divided
N_{disch} :	equal to 1 if there are no CHARGING segments in the mission
np_bat	number of battery cells in parallel
$n_{s,bat}$	number of battery packs in series
$N_{segm,piece}$	the number of segments of the mission piece "j".
P_{bat}	power required to the battery
P_{ice}	power required to the engine
Pice_n	engine nominal power
P_{mot}	power required to the motor
Pmot_n	motor nominal power
Pprop_vect	vector of required power at each mission phases
t	time vector containing the time length of each mission segment.

U	power-split ratio between motor and engine
V_bat	battery volume
V_ice	engine volume
V_mot	motor volume
V_tot	powertrain overall volume
V_vector	vector of mission phases speed
Vbus	battery nominal voltage
V_{cell}	the individual battery cell voltage from Kokam’s database.
vol_en_dens	battery volumetric energy density
z_vect	vector of mission phases altitude